Pol. J. Environ. Stud. Vol. 33, No. 1 (2024), 847-857
DOI: *10.15244/pjoes/172026* ONLINE PUBLICATION DATE: 2023-11-06

Original Research

Landslide Hazard Risk Assessment Based on Disaster Bearing Body: a Case Study of Heitai Landslide Group in Yongjing County, Gansu Province

Xuan Song[1]*, Peng Yang[2]

[1]College of Geosciences and Engineering, North China University of Water Resources and Electric Power, Zhengzhou 450045, China
[2]Shanghai Urban Construction Design & Research Institute (Group) Co., Ltd., Shanghai 200125, China

Received: 18 July 2023
Accepted: 8 September 2023

Abstract

Landslides pose a huge threat to human safety and infrastructure, and quantitative risk assessment of landslide disasters is of great significance for regional geological disaster prevention and control. In this study, there is an undeniable distance issue between the development area of landslides and the disaster bearing body based on a large scale. Based on this, the concept of disaster bearing capacity was proposed, and a landslide disaster risk assessment method with disaster bearing bodies as the research object was ultimately constructed. Taking the geological conditions of the Heitai landslide group as the research object, the impact range of the landslide under different working conditions on the east and south sides was determined using Massflow software, and the disaster bearing bodies within the impact range were divided into fishing nets using GIS technology. Each fishing net was endowed with life value and economic value, and landslide risk assessment was conducted on the east and south sides of Heitai. The results indicate that the study area has 57.3%, 14.2%, 18.1%, and 10.4% of extremely high, high, medium, and low disaster bearing areas, respectively. The extremely high, high, medium, and low risk areas in this region account for 12.9%, 15.8%, 22.2%, and 49.1% respectively. The proportion of extremely high, high, medium, and low risk areas in the economy is 7.1%, 23.2%, 15.6%, and 54.2%, respectively. The risk quantification method proposed in this article can provide a theoretical basis for landslide disaster warning.

Keywords: disaster bearing body, landslide disasters, risk assessment, Heitai landslide group

*e-mail: academicsx@163.com

Introduction

On a global scale, landslides pose a huge threat to human safety and the normal operation of infrastructure [1-4]. Meanwhile, due to the deteriorating global extreme climate and its impact on the geological environment, the harm of landslides will further expand [4-8]. China is one of the countries with the most frequent landslides in the world. According to relevant statistics, a total of 3919 landslide disasters occurred in 2022, accounting for more than half of the total geological disasters. This not only caused significant economic losses, but also caused huge casualties and suffering. On April 4, 1997, a large-scale Karst Plateau landslide occurred in Tongren City, Guizhou Province, China, causing 108 deaths. Two years later, another Prefecture-level city in Guizhou Province experienced a landslide, causing an astonishing number of 168 deaths [9]. In 2011, a landslide occurred at the Bailuyuan Dam in Xi'an, Shaanxi Province, resulting in 32 deaths [10]. In 2019, a landslide occurred in Xiangchu County, Linfen City, Shaanxi Province, causing 20 deaths and 13 injuries [11]. Landslides can not only directly cause harm to human society, but also trigger secondary disasters such as tsunamis. On December 21, 2004, an underwater landslide in Indonesia directly caused a large-scale tsunami in the local waters, resulting in casualties and damage to economic buildings [12-14]. From this perspective, the harm of landslides to human society is enormous, therefore, it is necessary to conduct risk assessment of landslide disasters.

Risk assessment, as one of the important tools for landslide prevention and reduction, has never stopped the research on risk assessment by domestic and foreign scholars [15-19]. Yao et al., [20] drew the landslide sensitivity map based on the landslide sensitivity depth neural network model of Semi-Supervised Learning. Nguyen and Kim [21] used statistical and physical models to estimate landslide hazards and calculated landslide risk indices based on vulnerability values and landslide risk indices. Riaz et al., [22] used the Random forest model to analyze the spatial probability of landslide sensitivity, and used the Poisson Statistical model to analyze the temporal probability of landslide disaster.

According to the different scales of landslide risk assessment, it can be divided into four scales, namely national scale (scale<1:250000), regional scale (scale<1:250000), site scale (scale<1:25000), and individual scale (scale>1:5000) [23]. The existing content of landslide risk assessment mainly includes risk assessment, vulnerability assessment of disaster bearing bodies, and value assessment [24]. Landslide risk assessment has undergone more than 40 years of development and progress, and it has become an essential work in landslide disaster prevention and reduction.

In order to further study and put forward a more comprehensive and accurate landslide risk assessment, this paper proposes the concept of disaster bearing capacity and constructs a landslide disaster risk assessment method based on the disaster bearing body as the research object. The object of this study is landslide risk assessment at the single scale. Firstly, the impact range of landslides under different working conditions was determined using Massflow software, and then GIS technology was used to divide the disaster bearing bodies within the impact range into fishing nets to evaluate their life value and economic value. The landslide hazard risk assessment proposed in this paper has been applied to the Heitai landslide group, and the landslide risk assessment has been conducted on the east and south sides of the Heitai area.

Risk Assessment Methods

Proposing the Concept of Disaster Tolerance

The individual scale landslide risk assessment, as the largest and most accurate individual scale landslide risk assessment, is undoubtedly the key to scientific disaster prevention and reduction guidance in the research area. However, the current mainstream landslide risk assessment methods seem to overlook the distance between the development point of landslide disasters and the location of the disaster bearing body at the individual scale. In fact, the location of landslide development areas and disaster bearing bodies in individual scale risk assessment is different, which will greatly compromise the applicability and accuracy of landslide risk assessment methods at individual scale.

Disaster bearing bodies refer to human social entities directly affected and damaged by disasters [15, 25, 26]. To accurately describe the possibility of the disaster bearing body suffering from landslide disasters, this paper proposes the concept of disaster bearing capacity. Disaster bearing capacity refers to the likelihood that a disaster bearing body within a certain area will experience landslide disasters within a certain period of time, and its value is related to the location of the disaster bearing body and the susceptibility of landslide disasters. The higher the disaster tolerance, the greater the likelihood of the disaster bearing body suffering from landslide disasters. The proposal of disaster bearing capacity can reflect the possibility of landslide causing harm to the disaster bearing body in every part of the disaster bearing body through its different positions, thus enabling the fine landslide risk assessment work at the individual scale to proceed smoothly.

Steps for Disaster Tolerance Evaluation

The evaluation of disaster tolerance can be divided into three steps, which are applicable to situations where the distance between the landslide development area

and the disaster bearing body cannot be ignored under the scale of individual landslide risk assessment. The steps for disaster tolerance evaluation are as follows:

(1) Investigation of landslide inducing factors

Based on the terrain, topography, geological structure and other factors studied, the main control factors for landslide induction in the region are selected, such as precipitation, irrigation, earthquakes, etc. Precipitation can saturate the soil, and when the soil is saturated, water fills the pore space of the soil, reducing the cohesion of the soil. This makes the soil unstable and prone to landslides. Improper irrigation can cause soil to oversaturate, especially if the irrigation water above the slope can penetrate the slope and increase soil saturation. When irrigation water is stuck on slopes, it also makes the soil unstable and increases the likelihood of landslides. Earthquakes produce violent surface movements that can lead to the fragmentation and rearrangement of soil. In addition, earthquakes can cause the water table to rise, further increasing soil saturation. Under the risk assessment of individual scale landslides, the triggering factors of landslides are relatively single compared to the site scale and regional scale, and the triggering factors are easier to calculate.

(2) Select evaluation scope

Calculate the extreme working conditions in the study area, namely the most unfavorable working conditions for landslides under natural or historical conditions, using a three-dimensional model. Under this working condition, the impact range of the landslide will reach its maximum, and the landslide impact range corresponding to the extreme working condition is the research scope of landslide risk assessment. Calculate the most critical conditions for inducing landslides within the research area, such as selecting a certain elevation of groundwater level for landslides induced by groundwater level rise. If the groundwater level reaches this level, it is easy to trigger landslides, and if it cannot reach this height, it is difficult to generate landslides. The disaster bearing body within the corresponding impact range under critical and extreme operating conditions is both the object of risk assessment.

Using the improved MacCormack-TVD finite difference method for numerical calculations, the conversion of geological models to numerical models at different computational levels is achieved. Then, based on the conservation of mass and momentum equations, the physical quantities in the Navier-Stokes equation are integrated along the Z-direction. Without considering the erosion and surge of pore water during landslide movement, the Coulomb model was selected for parameter inversion calibration. The shear strength and soil pressure of the flowing and sedimentary layers are shown in Equations (1-4).

$$\frac{\partial h_1}{\partial t}+\frac{\partial h_1 u_1}{\partial x}+\frac{\partial h_1 v_1}{\partial y}=0 \tag{1}$$

$$\frac{\partial(\rho_1 \mathrm{h}_1 u_1)}{\partial t}+\frac{\partial\left(\rho_1 \mathrm{h}_1 u_1^{\,2}\right)}{\partial x}+\frac{(\rho_1 \mathrm{h}_1 u_1 v_1)}{\partial y}$$
$$=\rho_1 u_1(Z_{1bot})E_{1bot}-\tau_{1zxbot}-\rho_1 g h_1\frac{\partial(h_1+Z_{1bot})}{\partial x} \tag{2}$$

In the equation, ρ_1 and h_1 represents the density and thickness of flow layer No. 1, while u_1 and v_1 represent the boundary velocities in the x and y directions, τ_{1zxbot} is the shear stress of the upper flow layer to the bottom, Z_{1bot} is the base boundary of the top flow layer, E_{1bot} is the entrainment rate of the bottom stable layer, and g is the gravitational acceleration.

$$\tau=\mathrm{c}+(1-\lambda\varphi)ght\tan\varphi \tag{3}$$

$$k_{ap}=\frac{2}{\cos^2\varphi}\times\left[1\pm\sqrt{1-(1+\tan^2\delta)\cos^2\varphi}\right]-1 \tag{4}$$

In the equation, c is the cohesion force, φ is the internal friction angle, λ is the coefficient of excess pore water pressure, ρ is the material density, g is the gravitational acceleration, h is the layer thickness in the vertical direction, δ is the base friction angle.

(3) Disaster tolerance evaluation

Based on the specific situation of the research area and the classification criteria for risk assessment, a certain number of intermediate conditions with suitable intervals will be set between extreme and critical conditions. Select the number of intermediate conditions between control and extreme conditions based on the accuracy requirements of risk assessment, and then delineate disaster bearing zones based on the corresponding impact range of each type of industrial control.

Method for Evaluating the Value of Disaster Bearing Bodies

The value of disaster bearing bodies includes life value and economic value. The evaluation of life value is based on population density and the temporal distribution of population within each grid. The evaluation of economic value is carried out using a weighted information model. The weighted information model comprehensively considers the differences in the impact of different influencing factors on the economic value of the disaster bearing bodies, and uses the Analytic Hierarchy Process to assign weight to the information value. Using numbers 1-9 and their reciprocal as scales, construct a judgment matrix, and conduct qualitative and quantitative analysis on this basis to determine the weights of different evaluation factors.

To avoid interference from other factors on the results and ensure the accuracy of the judgment matrix, the consistency index *CI* value is used to test the results.

Table 1. Average random consistency index *RI* values.

Degree	1	2	3	4	5	6	7	8	9	10
RI	0.00	0.00	0.52	0.89	1.12	1.26	1.36	1.41	1.46	1.49

When n>3, the consistency index *RI* is introduced, and the values are shown in Table 1. *CR*<0.1 indicates that the judgment matrix has passed the consistency test.

$$CI = \frac{\lambda_{\max} - n}{n-1} \tag{5}$$

$$CR = \frac{CI}{RI} \tag{6}$$

In the equation, λ_{max} is the maximum eigenvalue of the judgment matrix; n is the order of the judgment matrix.

Model Application

Description of the Test Area

In this study, the Heitai landslide group in Yongjing County of Gansu Province is used to solve the landslide hazard risk assessment of the disaster bearing body as the research object. Heitai is located in Yongjing County, Gansu Province. The west side is separated by the Tiger Wolf Valley, the north side is cut by the Moshi Valley, the south and east sides are terrace terraces, and the Yellow River and Huangshui River meet here. The black platform covers an area of about 9 km^2, with relatively small differences in lithology and is roughly distributed in an east-west strip shape, with narrow east-west ends. The widest point in the middle is about 3 km, and the tabletop is open and flat. Gently dipping from west to east, with a slope generally of 3-10°. This region is located in the northwest inland area of China, belonging to the temperate semi-arid climate, less precipitation, large evaporation, dry climate. The average annual precipitation is 287.6 mm, the average annual evaporation is 178.8 mm, and the precipitation concentration is high, 70%~80% of the precipitation is concentrated in July, August and September, and most of it is heavy rain. In winter, the cold period reaches 180 d, the average temperature is minus 3.4ºC, the freezing period generally begins in late November, and the thaw begins from late February to early March of the following year, and the average maximum freezing depth is 0.92 m. The stratum of the Yellow River Class IV terrace is relatively simple and there is no strong tectonic geological movement around it. According to the surface exposure and drilling exposure of the black platform, the black platform can be divided into 4 stratigraphic units from top to bottom:

(1) Upper Pleistocene eolian loess layer. The thickness of this formation ranges from 30 to 50 meters, mainly in a grayish yellow color, mainly composed of silt particles. The soil composition is uniform, loose and porous, with a large number of vertical cracks developed. The Jiaojia section on the east side of the plateau and the Moshigou section on the north side are thicker, while the Hulanggou section on the west side of the plateau and the Dangchuan section on the south side of the plateau have a thinner loess layer, which is generally higher in the east and lower in the west.

(2) Middle Pleistocene silty clay layer. The thickness of this layer ranges from 3 to 20 meters, mainly in a reddish brown color, with horizontal joints and relatively poor water permeability. After irrigation water reaches this layer through vertical cracks, it is difficult to continue to penetrate, forming a natural water barrier.

(3) Middle Pleistocene sandy pebble layer. The thickness of this formation ranges from 1 to 9 meters, and it is mainly grayish white with good roundness. It is exposed near Jiaojia Village on the east side of the plateau, and sporadic on the south side of the plateau.

(4) Lower Cretaceous Hekou Group sandstone mudstone interbedding. The stratum is brownish brown and brownish red, mainly composed of mudstone, and mixed with thin Siltstone. The exposed position of the surface layer is severely weathered, and the joint fissures are relatively developed. The rock stratum inclines to the southeast direction. The two groups of main joint directions are NE65°∠72° and NW335°∠65°.

Due to drought and limited rainfall, and the lack of groundwater formation on the Black Terrace itself. In the 1950s and 1960s, immigrants from Liujiaxia, Bapanxia, and Yanguoxia reservoir areas settled here. In order to meet the needs of residents' daily life and agricultural irrigation, a large-scale water diversion irrigation project was completed in 1964. In the past 30 years, the annual irrigation volume has been maintained at over 500×10^3 m^3, which has directly led to the formation and annual increase of groundwater in the Heifangtai area, leading to frequent landslides. At present, the landslide has caused direct economic losses of over 400 million yuan, resulting in 37 deaths and over 100 injuries. 450 households have been affected in their daily lives, with nearly 12.14 km^2 of farmland destroyed and roads leading to Yanguoxia Chemical Plant and Yanguoxia Power Plant buried multiple times, affecting 4 schools and 13 enterprises [27].

Assessment of Disaster Bearing Capacity of Disaster Bearing Bodies

Determination of Research Scope and Division of Fishing Nets

The disaster bearing body is the residents, houses, workshops, roads, communication and power facilities, crop planting areas, etc. within the scope of the impact of the mass landslides in the east and south of Heitai. The disaster bearing body on the east and south sides of the Heitai plateau is adjacent to the Yellow River, so the risk assessment is between the plateau and the Yellow River, with an area of approximately 4.02 km^2. The fishing net division function of GIS is used to divide the affected areas into 20×20 m fishing nets, covering a total of 6916 effective fishing nets. A single fishing net is the basic unit for this landslide risk assessment (Fig. 1).

Calculation of Landslide Impact Range

Large area irrigation on the loess plateau in the Heitai area can lead to an increase in the groundwater level in the loess phreatic aquifer, resulting in a significant decrease in the shear strength of the loess in the infiltration zone [28, 29]. This is the main controlling factor for the occurrence of landslides. Due to the good permeability of the pebble layer at the bottom of the silty clay in the Heitai area, the water that seeps into this layer can be discharged in the form of springs at the edge of the plateau [27], so the underground water level in Heitai cannot rise unrestricted. When the groundwater level reaches a depth of 15 m, the sum of precipitation and irrigation infiltration in the Heitai area cannot further raise the groundwater level. Therefore, a groundwater depth of 15 m is the extreme condition for controlling landslides in the Heitai area. When the groundwater depth is higher than 30 m, the overall stability coefficient of Heitai Plateau is higher (all greater than 1), and the possibility of landslides is lower. Therefore, a groundwater depth of 30 m is the control water level that causes landslides in Heitai Plateau. Finally, four working conditions with groundwater depths of 30 m, 25 m, 20 m, and 15 m were selected for numerical simulation calculation of the movement process of the Heitai Plateau landslide.

Based on the physical and mechanical parameters of rock and soil conducted on the Heitai platform [30], the cohesion, effective internal friction angle, and residual internal friction angle of rock and soil under water saturation were obtained through triaxial and ring shear experiments, with values of 0.81-6.65 kPa, 30.66°, and 30.5°-32.9°, respectively. At the same time, drawing on Massflow's numerical simulation inversion experiment, it was found that the cohesion c and excess pore water pressure coefficient λ It has a major impact on the shape and thickness of landslide accumulation. Horton et al., [31] used Massflow to study the initial release of debris flow h and excess pore water pressure λ through sensitivity analysis, it was found that λ plays a dominant role in the final accumulation and movement range of debris flow. After the landslide in the Heitai area loses stability, it may have a scraping erosion effect on the slope toe, which has a significant impact on the energy dissipation during the landslide movement process. When using Massflow inversion calculation and danger range prediction, cohesion c, base friction

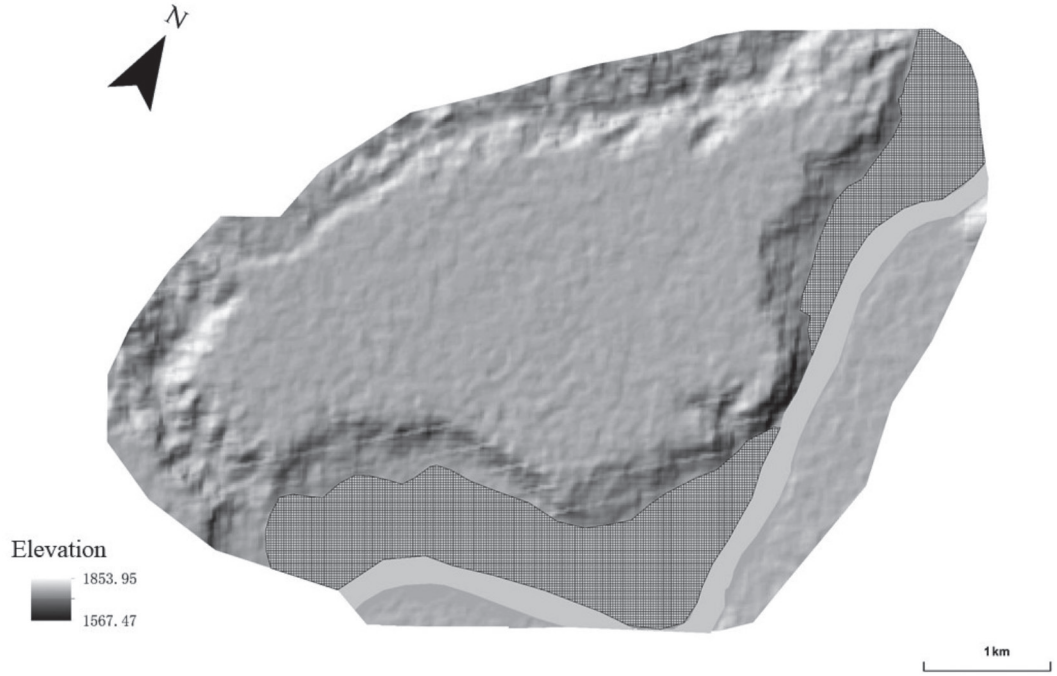

Fig. 1. Research scope and fishing net division effect diagram.

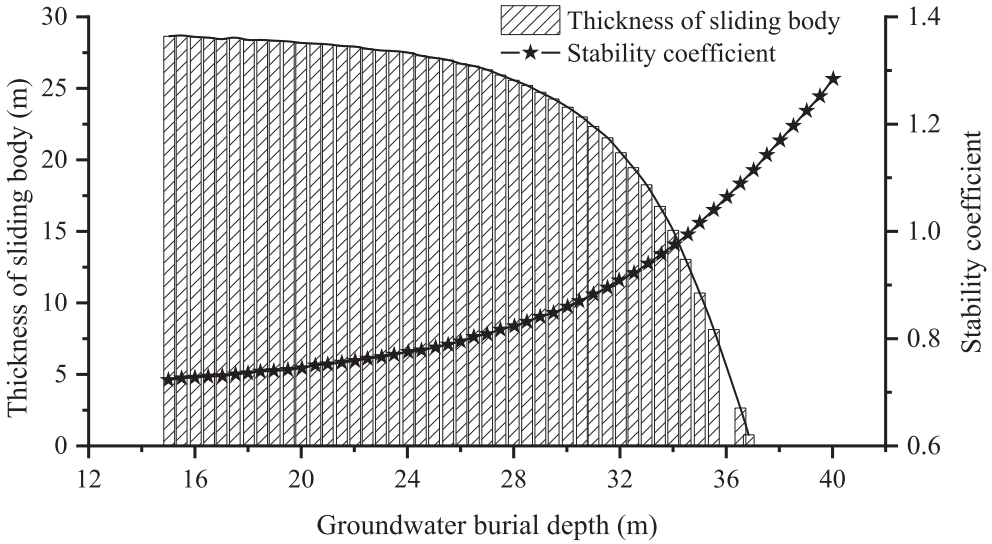

Fig. 2. Relation between groundwater level, landslide stability and slide thickness.

angle δ and excess pore water pressure coefficient λ may have differences in different time and space. However, the current numerical calculations cannot take it into account. Therefore, after balancing the model accuracy and computational complexity, this paper maintains the pore water pressure coefficient λ = 0.0-0.9, base friction angle δ = 0-30°, density of rock and soil mass ρ = 1400 kg/m^3, cohesion c = 1000 kPa, internal friction angle φ = 30.5° and calculation time t = 400 s, ensuring consistency of non-critical parameters in inversion analysis and simulation prediction. Through numerical simulation calculations of landslides on the east and south sides of Heitai, the stability of the landslide and the variation of landslide thickness with groundwater level as shown in Fig. 2 were obtained. As the groundwater burial depth decreases, the impact range of the landslide on the east and south sides of Heitai gradually increases, and the bulking thickness of the landslide after sliding also increases exponentially.

Results of Disaster Bearing Zoning

Fig. 3 shows that under four working conditions, the impact range of the landslide on the eastern and

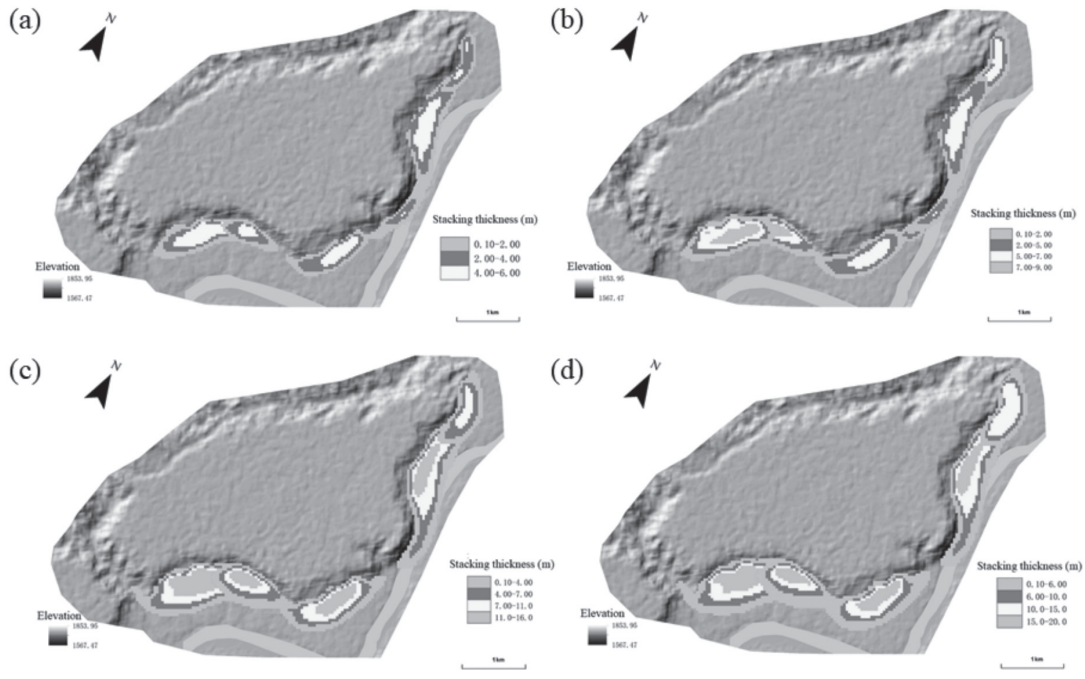

Fig. 3. Scope of landslide impact under different working conditions a) Groundwater depth of 30 m b) Groundwater depth of 25 m c) Groundwater depth of 20 m d) Groundwater depth of 15 m.

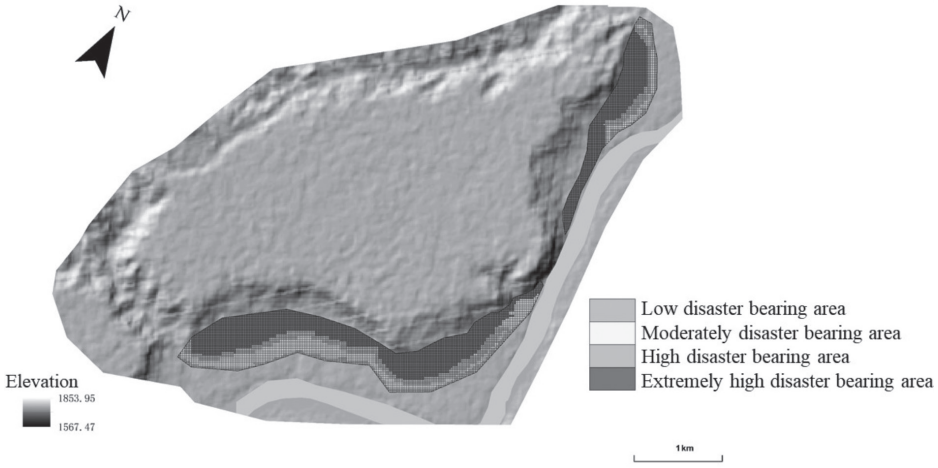

Fig. 4. Disaster bearing zoning map.

southern sides of the Heitai Plateau decreases with the increase of groundwater burial depth. Therefore, based on the sliding range corresponding to the four working conditions, the disaster bearing body in the area is divided into disaster bearing zones. The landslide impact area corresponding to a groundwater depth of 30 m is an extremely high disaster bearing area, while the landslide impact area corresponding to a groundwater depth of 25 m is a high disaster bearing area except for the extremely high disaster bearing area. By analogy, the areas far from the plateau are classified as medium disaster bearing areas and low disaster bearing areas in sequence. The disaster tolerance of a single fishing net is divided based on its location, as shown in Fig. 4. Among them, there are 3964 extremely high disaster bearing fishing nets, accounting for 57.3%; 982 high disaster bearing fishing nets, accounting for 14.2%; 1253 medium disaster bearing fishing nets, accounting for 18.1%; 717 low disaster bearing fishing nets, accounting for 10.4%.

Results

Assessment of the Life Value of the Disaster Bearing Body

According to official data such as the 7th National Population Census, the research area includes five natural villages: Xinyuan Village, Sansheng Village, Huangci Village, Chenjia Village, and Jiaojia Village, with a population density of approximately 91.2 people/km^2. Based on on-site investigation and experience, the average annual working time of crops in this area is about 929.8-981.2 hours, and the average indoor stay

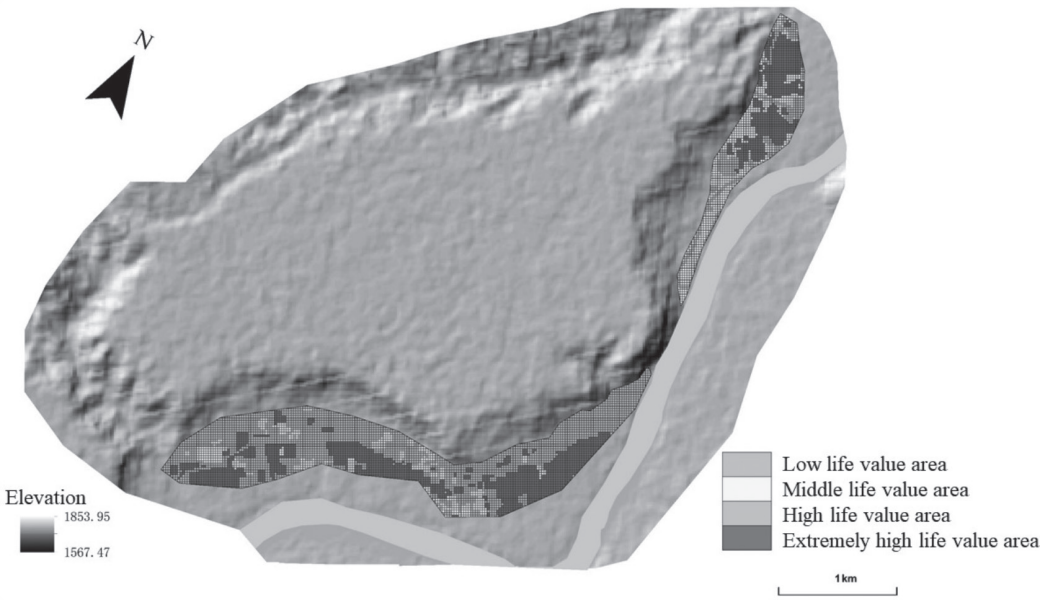

Fig. 5. Life value division results.

time of residents is about 5470 hours. Assuming that all time except for labor and indoor time is spent outdoors in other areas, the spatiotemporal probabilities of local residents in houses, farmland, and other areas are 62.50%, 11.41%, and 26.09%, respectively. Fig. 5 shows the results divided into extremely high life value area, high life value area, medium life value area, and low life value area based on the natural discontinuity method.

Economic Value Evaluation of Disaster Bearing Bodies

Based on the types and characteristics of disaster bearing bodies in the region, four types of houses, roads, crops, and vacant land were selected for economic value grading and assignment. The grading standards are shown in Table 2.

Based on the Analytic Hierarchy Process, select the disaster bearing bodies in the region to construct a judgment matrix, and quantitatively analyze the economic value of the disaster bearing bodies. The weight values are shown in Table 3.

Perform consistency check according to Equations (5-6) to obtain the maximum eigenvalue of the judgment matrix $\lambda_{max} = 4.0716$, random consistency ratio $CR = 0.0268<0.10$, and through consistency testing, the distribution of weight coefficients is reasonable. For different types of disaster bearing bodies, stack them according to Equation (7).

$$V = \sum_{i=1}^{n} Weight_i \bullet X_i \tag{7}$$

In the formula, V represents economic value; $Weight_i$ is the weight value of the disaster bearing body; X_i is the assigned value for each level.

Fig. 6 shows the results divided into four categories based on the natural discontinuity method: extremely

Table 2. Classification criteria for economic value evaluation factors of disaster bearing bodies.

Factor	Assignment					
	0.1	0.2	0.3	0.4	0.5	0.6
Building structure type	Barrack	Single layer fired brick mixed structure	Double layer and above brick concrete structure	Single layer concrete structure	Double layer concrete structure	Concrete structure above double layer
Road type	Dirt road	Cement road	Asphalt road	—	—	—
Usage of vacant land	Abandoned farmland	Stacking of building materials	Crop drying	—	—	—
Crop type	Annual vegetables	Annual corn	Perennial jujube tree	Perennial apples	—	—

Table 3. Judgment matrix and weights of economic value evaluation factors for disaster bearing bodies.

	Road	House	Crops	Space	Weight
Road	1	2	3	3	0.4495
House	1/2	1	2	2	0.2596
Crops	1/3	1/2	1	2	0.1707
Space	1/3	1/2	1/2	1	0.1202

Table 4. Landslide risk grading evaluation matrix based on the value and tolerance of disaster bearing bodies.

Value	Disaster tolerance			
	Extremely high disaster tolerance	High disaster tolerance	Medium disaster tolerance	Low disaster tolerance
Extremely high valuable	Extremely high risk	Extremely high risk	High risk	Medium risk
High value	Extremely high risk	High risk	High risk	Medium risk
Medium value	High risk	High risk	Medium risk	Low risk
Low value	Medium risk	Medium risk	Low risk	Low risk

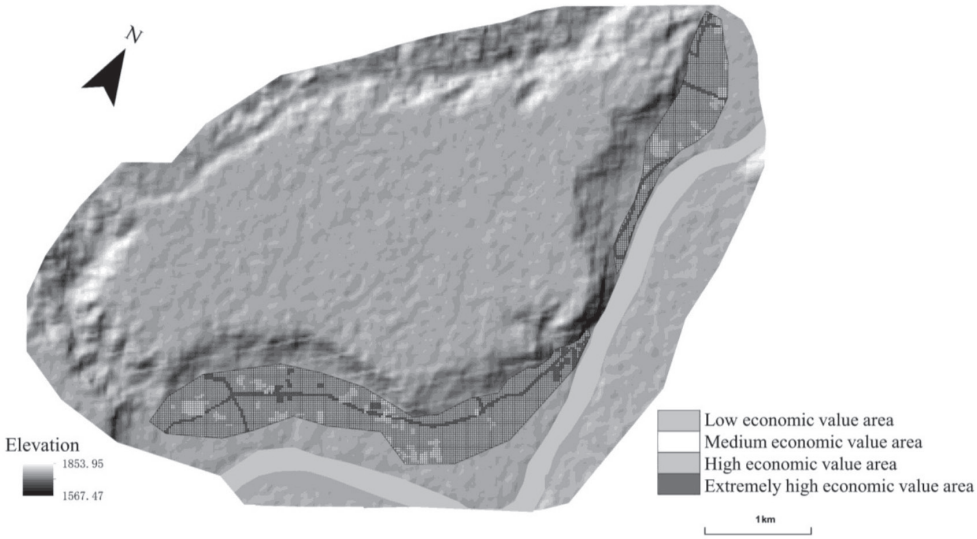

Fig. 6. Economic value division results.

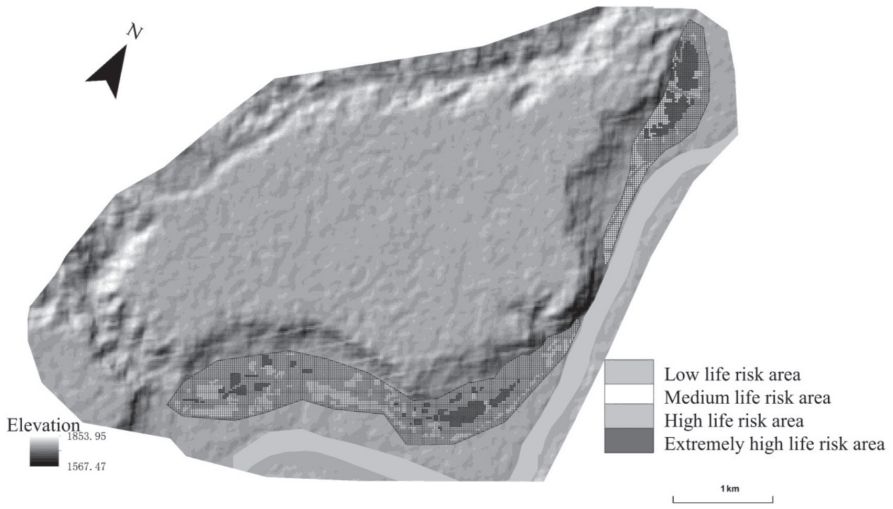

Fig. 7. Life risk assessment results of disaster bearing bodies.

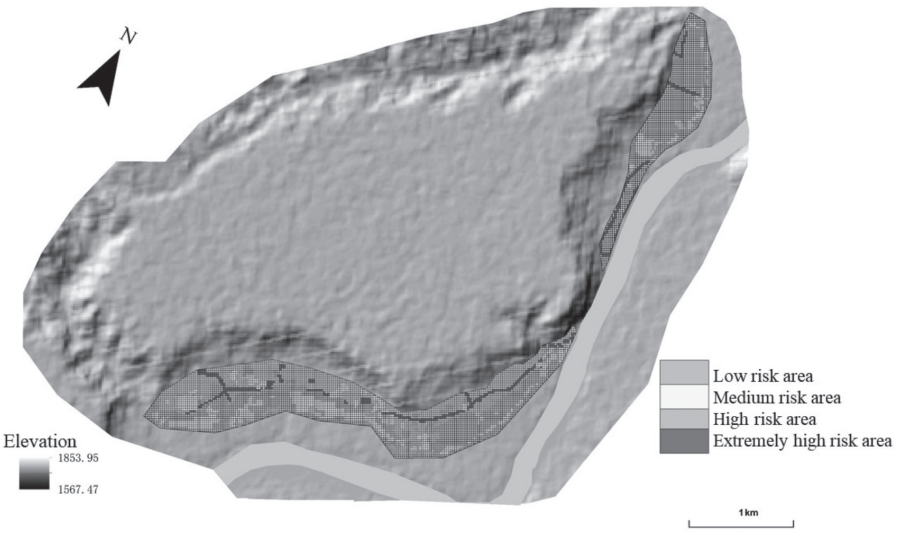

Fig. 8. Economic risk assessment results of disaster bearing bodies.

high economic value zone, high economic value zone, medium economic value zone, and low economic value zone.

Risk Assessment of Disaster Bearing Bodies

Based on the theory of risk assessment matrix, a landslide risk grading evaluation matrix based on the value and disaster bearing capacity of the disaster bearing body is constructed (Table 4). Based on the disaster bearing capacity, life value, and economic value of each fishing net, the grid calculator function of GIS technology is used to fuse information on the disaster bearing capacity, life value, and economic value of each fishing net, and to classify the risk. The division results are shown in Fig. 7 and Fig. 8.

The evaluation results indicate that there are 892 extremely high risk fishing nets in the area, accounting for 12.9%; 1094 high risk fishing nets, accounting for 15.8%; 1537 medium risk fishing nets, accounting for 22.2%; There are 3393 low risk fishing nets, accounting for 49.1%. The first proportion of life risk in this region is low risk and the second proportion is medium risk. 485 fishing nets with extremely high economic risks, accounting for 7.1%; 1602 high risk fishing nets, accounting for 23.2%; 1078 medium risk fishing nets, accounting for 15.6%; 3751 low risk fishing nets, accounting for 54.2%. The first proportion of economic risk in this region is low risk and the second proportion is high risk. From the results of the life risk assessment (Fig. 7), it can be seen that in the northern region, due to the concentration of villages compared to the southern side and the relatively small distance from the plateau, the proportion of extremely high risk areas in the northern region is much higher than that in the southern region. From the results of economic risk assessment (Fig. 8), it can be seen that most of the roads in the study area are located in areas with extremely high disaster tolerance and high disaster tolerance, resulting in most of the economically high risk areas being distributed along the roads.

When the groundwater level is high, there is a greater risk of disaster in the east and south of the black platform. It is suggested that the irrigation quantity should be reduced under the premise of meeting the demand of agricultural irrigation and the situation of flood irrigation should be prevented as far as possible. According to the life and economic risks of disaster victims, corresponding disaster prevention and mitigation measures are made. At the same time, strengthen the geological disaster education measures, strengthen the mass prevention and control system, reduce the loss caused by landslides.

Conclusions

According to the characteristics of landslide risk under large scale, the concept of disaster bearing is proposed in this paper. Taking the Heitai landslide group as an example, a landslide risk assessment model based on disaster bearing bodies has been established, which solves the problem of refined landslide risk assessment at large scales and provides new ideas for landslide risk assessment. The impact range of the Heitai Group landslide at different groundwater depths was obtained, and based on this, the disaster bearing body was zoned.

The study area has 57.3%, 14.2%, 18.1%, and 10.4% of extremely high, high, medium, and low disaster bearing areas, respectively. The types of disaster bearing bodies within each fishing net were counted, and based on this, the life value and economic value of fishing nets in extremely high, high, medium, and low disaster bearing areas were assigned, and their life risk and economic risk were calculated. The results showed that the areas with extremely high, high, medium, and low risk of life in the study area accounted for 12.9%, 15.8%, 22.2%, and 49.1%, respectively; The proportion of extremely high, high, medium, and low risk areas in the economy is 7.1%, 23.2%, 15.6%, and 54.2%.

Acknowledgments

This research is supported by the independent research and development project of Shanghai Urban Construction Design and Research Institute (Group) Co., Ltd. (CK2022018A).

Conflicts of Interest

The authors declare that they have no conflict of interest.

References

1. YAN J., KONG L., XIONG C., XU G. Damage Analysis of Shear Mechanical Behavior of Pile–Structural Soil Interface Considering Shear Rate Effect. Acta Geotechnica, **2023**. DOI: 10.1007/s11440-023-01912-6
2. SUI H., SU T., HU R., WANG D., ZHENG Z. Study on the Risk Assessment Method of Rainfall Landslide. Water, **14** (22), **2022**.
3. YAN J., KONG L., WANG J. Evolution Law of Small Strain Shear Modulus of Expansive Soil: From A Damage Perspective. Engineering Geology, **315**, **2023**.
4. TANG Y., CHE A., CAO Y., ZHANG F. Risk Assessment of Seismic Landslides Based on Analysis of Historical Earthquake Disaster Characteristics. Bulletin of Engineering Geology and the Environment, **79** (5), 2271, **2020**.
5. GAO Z., DING M., HUANG T., LIU X., HAO Z., HU X., CHUANJIE X. Landslide Risk Assessment of High-Mountain Settlements Using Gaussian Process Classification Combined With Improved Weight-Based Generalized Objective Function. International Journal of Disaster Risk Reduction, **67**, 102662, **2022**.

6. PACHUAU L. Zonation of Landslide Susceptibility And Risk Assessment in Serchhip Town, Mizoram. Journal of the Indian Society of Remote Sensing, **47** (9), 1587, **2019**.
7. AZIMI S.R., NIKRAZ H., YAZDANI-CHAMZINI A. Landslide Risk Assessment by Using A New Combination Model Based on A Fuzzy Inference System Method. KSCE Journal of Civil Engineering, **22**, 4263, **2018**.
8. SONG K., YANG H., LIU X., LIANG D., CHEN L. Risk Assessment on The Stability of Barrier Dam Induced by Caijiaba Landslide, SW China. Bulletin of Engineering Geology and the Environment, **81** (6), 235, **2022**.
9. HUANG M., QI S., SHANG G. Karst Landslides Hazard During 1940-2002 in the Mountainous Region of Guizhou Province, Southwest China. Natural hazards, **60**, 781, **2012**.
10. ZHUANG J.Q., PENG J.B. A Coupled Slope Cutting – A Prolonged Rainfall-Induced Loess Landslide: A 17 October 2011 Case Study. Bulletin of Engineering Geology and the Environment, **73** (4), 997, **2014**.
11. CUI Y., XU C., XU S., CHAI S., FU G., BAO P. Small-Scale Catastrophic Landslides in Loess Areas of China: An Example of The March 15, 2019, Zaoling Landslide In Shanxi Province. Landslides, **17**, 669, **2020**.
12. KELFOUN K., GIACHETTI T., LABAZUY P. Landslide-Generated Tsunamis At RÉUnion Island. Journal of Geophysical Research: Earth Surface, **115** (F4), **2010**.
13. MURILLO-GARCÍA F. G., ROSSI M., ARDIZZONE F., FIORUCCI F., ALCáNTARA-AYALA I. Hazard And Population Vulnerability Analysis: A Step Towards Landslide Risk Assessment. Journal of Mountain Science, **14**, 1241, **2017**.
14. PERRONE A., CANORA F., CALAMITA G., BELLANOVA J., SERLENGA V., PANEBIANCO S., TRAGNI N., PISCITELLI S., VIGNOLA L., DOGLIONI A. A Multidisciplinary Approach For Landslide Residual Risk Assessment: The Pomarico Landslide (Basilicata Region, Southern Italy) Case Study. Landslides, **18**, 353, **2021**.
15. MOSAFFAIE J., SALEHPOUR JAM. A., SARFARAZ F. Landslide Risk Assessment Based on Susceptibility And Vulnerability. Environment, Development and Sustainability, **1**, **2023**.
16. ALTHUWAYNEE O.F., PRADHAN B. Semi-Quantitative Landslide Risk Assessment Using GIS-Based Exposure Analysis in Kuala Lumpur City. Geomatics, Natural Hazards and Risk, **8** (2), 706, **2017**.
17. SUN J., ZHOU F. Stability And Support Analysis of Coverage Rock-Soil Aggregate of Longhuguan Landslide. Polish Journal of Environmental Studies, **26** (6), **2017**.
18. DAI F., LEE C.F., NGAI Y.Y. Landslide Risk Assessment And Management: An Overview. Engineering geology, **64** (1), 65, **2002**.
19. RAM P., GUPTA V. Landslide Hazard, Vulnerability, And Risk Assessment (HVRA), Mussoorie Township, Lesser Himalaya, India. Environment, Development and Sustainability, **1**, **2022**.
20. YAO J., QIN S., QIAO S., CHE W., CHEN Y., SU G., MIAO Q. Assessment of Landslide Susceptibility Combining Deep Learning With Semi-Supervised Learning in Jiaohe County, Jilin Province, China. Applied Sciences, **10** (16), **2020**.
21. NGUYEN B-Q-V., KIM Y-T. Regional-Scale Landslide Risk Assessment on Mt. Umyeon using risk index estimation. Landslides, **18** (7), 2547, **2021**.
22. RIAZ M.T., BASHARAT M., BRUNETTI M.T., RIAZ M.T. Semi-Quantitative Landslide Risk Assessment of District Muzaffarabad, Northwestern Himalayas, Pakistan. Stochastic Environmental Research and Risk Assessment, **1**, **2023**.
23. FELL R., COROMINAS J., BONNARD C., CASCINI L., LEROI E., SAVAGE W. Z. Guidelines for Landslide Susceptibility, Hazard And Risk Zoning for Land Use Planning. Engineering geology, **102** (3-4), 85, **2008**.
24. CROZIER M.J., GLADE T. Landslide Hazard And Risk: Issues, Concepts And Approach. Landslide hazard and risk, **1**, **2005**.
25. ZHANG Y., GUO J., CHE Z. Discussion on Evaluating The Vulnerability of Storm Surge Hazard Bearing Bodies In The Coastal Areas of Wenzhou. Frontiers of Earth Science, **9**, 300, **2015**.
26. XIE S., LIU W., YUAN Z., ZHANG H., LIN H., WANG Y. Integrated Risk Assessment of Waterlogging in Guangzhou Based on Runoff Modeling, AHP, GIS and Scenario Analysis. Water, **14** (18), 2899, **2022**.
27. ZHAO K., XU Q., LIU F., XIU D., REN X. Field Monitoring of Preferential Infiltration in Loess Using Time-Lapse Electrical Resistivity Tomography. Journal of Hydrology, **591**, 125278, **2020**.
28. GU T.F., ZHANG M.S., WANG J.D., WANG C.X., XU Y.J., WANG X. The Effect of Irrigation on Slope Stability in the Heifangtai Platform, Gansu Province, China. Engineering geology, **248**, 346, **2019**.
29. CHEN Y., TANG L., YE Y., CHENG Z., ZHOU Z. Effects of Different Chloride Salts on Granite Residual Soil: Properties And Water–Soil Chemical Interaction Mechanisms. Journal of Soils and Sediments, **23** (4), 1844, **2023**.
30. FENG L., ZHANG S., JIN Z., ZHANG M., SUN P., JIA J., CHU G., HU W. The Critical Mechanics of The Initiation of Loess Flow Failure And Implications for Landslides. Engineering Geology, **288**, 106165, **2021**.
31. HORTON A.J., HALES T.C., OUYANG C., FAN X. Identifying Post-Earthquake Debris Flow Hazard Using Massflow. Engineering Geology, **258**, 105134, **2019**.